A Length-Scale Analysis of Instabilities in High Pressure Explosion Flames

R.D. Lockett*, R. Morishima
School of Engineering & Mathematical Sciences, The City University, London, EC1V 0HB, United Kingdom
*Corresponding author
Email: r.d.lockett@city.ac.uk

Abstract

Cellular flame structure in high pressure iso-octane-air explosion flames, obtained in the Leeds combustion bomb, was investigated using Schlieren cinematography and OH laser induced fluorescence. High pressure, stoichiometric, iso-octane-air explosion flames were observed to develop a relatively large wavelength cellular structure (3 mm to 7 mm) as a result of the Darrius-Landau hydrodynamic instability. High pressure, rich, iso-octane-air explosion flames (ϕ = 1.4) were observed to develop a cellular structure with two distinct wavelengths present on the flame surface, a large wavelength cellular structure that was comparable with before (3 mm to 7 mm), and a smaller wavelength cellular structure (~ 1 mm). It is suggested that the small wavelength cellularity is caused by the thermal-diffusive instability. It is further suggested that at high pressures, the hydrodynamic instability and the thermal-diffusive instability decouple from each other, resulting in a dual wavelength cellularity.

Keywords

Spherical explosion flame, flame instability, hydrodynamic instability, thermal-diffusive instability, cellular flame, cellular wavelength, length-scale, Schlieren cinematography, laser induced fluorescence, laser diagnostics.

1. Introduction

If a deformation occurs in the surface of a spherically expanding laminar flame during its early development, any potential instabilities (hydrodynamic, thermal-diffusive) will be stabilised by the flame stretch until a critical Peclet number is reached. After this critical point, the flame may become unstable to surface perturbations, which can grow on the flame surface through the development of propagating cracks and cellular fission [1].

If the Lewis number for the deficient reactant in the fuel-air mixture is below a critical value, then in general, a perturbation in the expanding flame front is unstable. This means that for fuel-air mixtures where the molecular mass of the fuel is considerably larger than the molecular mass of air, rich flames are unstable to surface perturbations. The converse is also true for lean flames. This kind of flame instability is known as a thermal-diffusive instability [1 – 3].

The second type of flame instability examined here is hydrodynamic in origin. Flame surface perturbations cause local pressure and density variations ahead of the advancing flame front, which can accelerate surface cracking. Hydrodynamic instabilities can be distinguished from thermal-diffusive instabilities through the identification of the different wavelengths associated with the two mechanisms [3]. In practice, initial perturbations in a spherically expanding flame surface occur as a consequence of the mode of ignition, whether by a spark plug, or laser, or other means [1 – 3].

This paper reports the results of experimental work conducted in the Leeds combustion bomb on high pressure iso-octane-air laminar explosion flames using Schlieren cinematography and OH laser induced fluorescence.

2. Experimental

2.1 The Leeds Combustion Bomb

The Leeds fan-stirred combustion bomb is a spherical vessel of volume 31 litres, with six 150 mm diameter optically accessible windows, and four tetrahedrally oriented high speed fans. The combustion chamber has an internal diameter of 39 cm, with 10 cm thick quartz windows. Ignition of flammable mixtures in the combustion volume can be achieved through the use of a centrally mounted spark plug, two spark plugs, or laser ignition.

A gas supply system involving oxygen, nitrogen, air and gaseous fuel is connected to the bomb to facilitate fuel-oxidant-inert mixing to any mixture strength and pressure. The proportions of the reactant gases are determined through measurement of the respective partial pressures. Liquid fuel can be introduced into the combustion volume using a syringe, and mixed with the oxidant and inert gases using the fans. Combustion experiments involving laminar explosion flames require a settled, stationary gaseous environment involving a homogeneous mixture of fuel and air. The fans may be used to mix the fuel and oxidant to achieve a homogeneous mixture, and are then turned off.

The laminar explosion flames were initiated from the centre of the bomb using single kernel spark plug ignition. Cellularity in spherically expanding laminar explosion flames was investigated for stoichiometric iso-octane-air flames and equivalence ratio $\phi = 1.4$ iso-octane-air flames at 5 bar pressure.

2.2 Schlieren Cinematography (conducted by R. Woolley, Univ. of Sheffield)

The Schlieren cinematography measurements were conducted by using a 15 cm diameter, 1 m focal length lens to collimate a white light source. The collimated beam was then passes through the bomb. A second 15 cm diameter, 1 m focal length lens was employed to focus the light past a knife edge located at the focus, and onto a high speed camera using a 50 mm focal length lens. The high speed camera obtained 756 x 756 pixel images with a frame rate of 1000 frames per second. The spatial resolution of the camera images were 0.256 mm per pixel [4].

2.3 Laser Induced Fluorescence Measurements

The OH planar laser induced fluorescence (PLIF) measurements were conducted in the Leeds bomb using a Lambda Physik EMG 150 MSC excimer laser, operating in narrow band tunable mode at 308.24nm. The rectangular laser pulses were formed into a 67 mm high sheet of width 0.2 mm, using a 2m focal length spherical lens and an inverted 4x cylindrical telescope. The resonance fluorescence obtained from the excited OH was imaged onto a lens coupled intensified CCD camera using a Nikon Nikkor 105 mm f4.5 uv grade fused silica lens. The spatial resolution of the fluorescence images were approximately 0.20 mm/pixel.

3. Results

Figure 1 shows a Schlieren image of a stoichiometric iso-octane-air spherical explosion flame obtained in the Leeds bomb at 5 bar pressure [3, 4]. The flame radius is approximately 60 mm. Surface wrinkling with a length-scale of approximately 3 mm to 7 mm is observable on the

flame surface, with a smooth surface between the wrinkle lines.

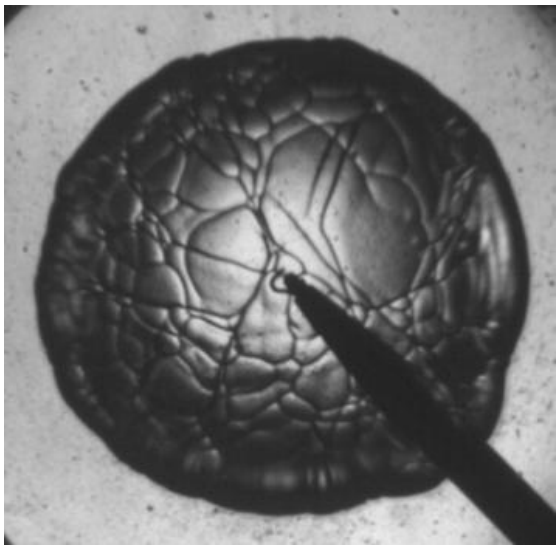

Figure 1: Schlieren image of a 5 bar, stoichiometric, iso-octane-air explosion flame [3, 4]. (Flame radii ≈ 60 mm).

Figure 2 shows a Schlieren image of a $\phi = 1.4$ iso-octane-air spherical explosion flame obtained in the Leeds bomb at 5 bar pressure [3, 4]. The flame radius is approximately 60 mm. Surface wrinkling with a length-scale range of approximately 3 mm to 7 mm is observable as before. In addition, there is a fine structure superimposed on the larger surface wrinkles.

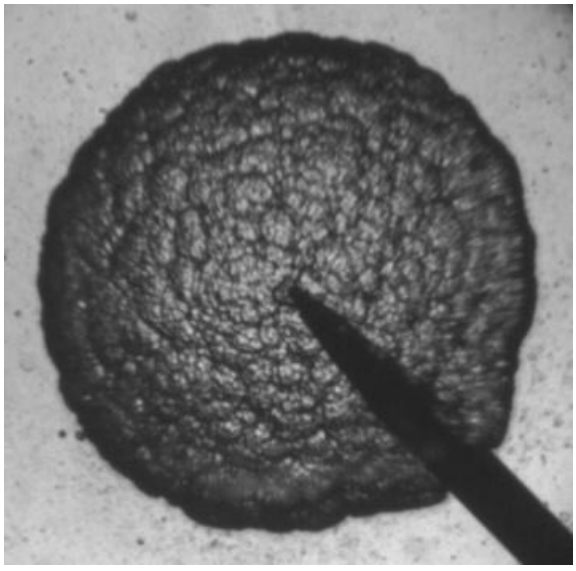

Figure 2: Schlieren image of a 5 bar, $\phi = 1.4$, iso-octane-air explosion flame [3, 4]. (Flame radius ≈ 60 mm).

The cellular structure visible in Figures 1 and 2 has been subjected to a length-scale analysis, which is presented in histogram form in Figures 3 and 4 below. These histograms indicate that the large cells observable in Figures 1 and 2 have very similar distributions, means and moments. The distribution of cell wavelengths shown in Figure 3 below has a mean and standard deviation of 5.9 mm and 3.1 mm respectively.

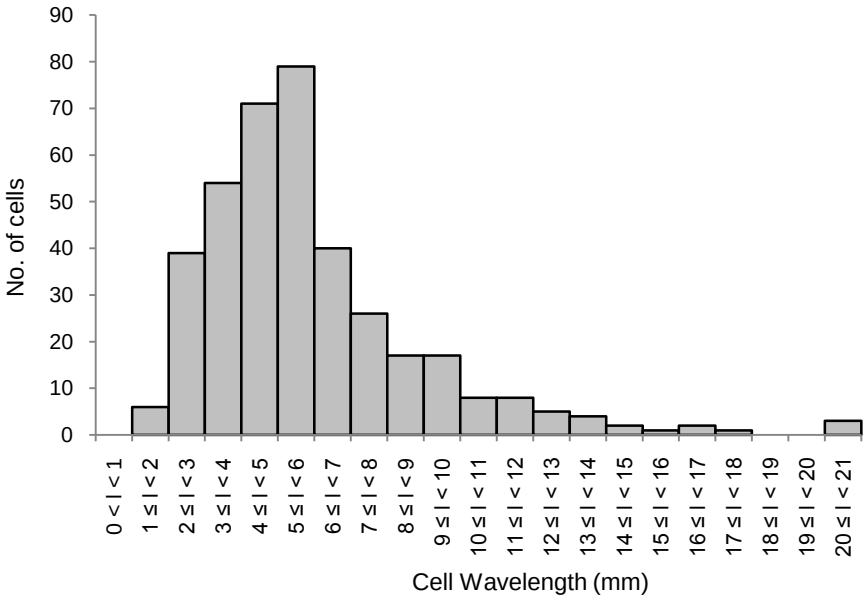

Figure 3: Histogram showing cell size distribution obtained from Figure 1.

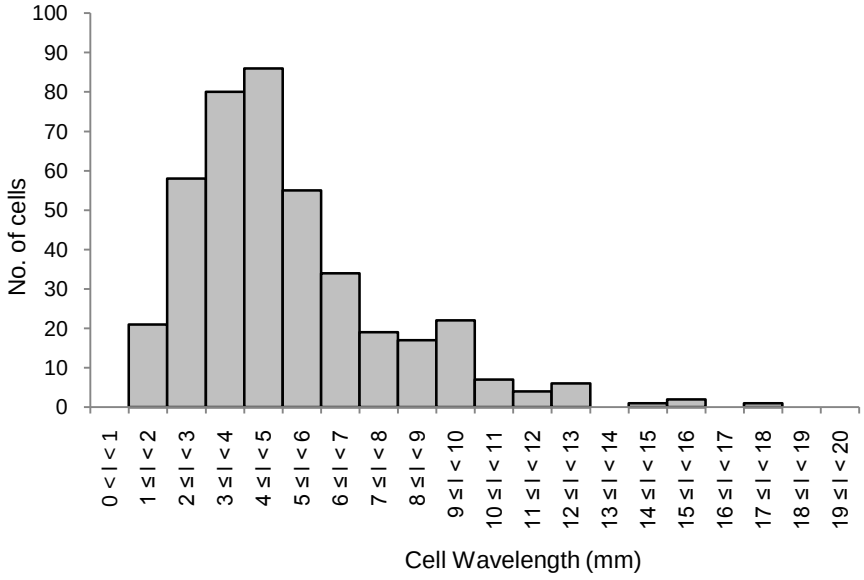

Figure 4: Histogram showing cell size distribution obtained from Figure 2.

The distribution of cell wavelengths shown in Figure 4 above has a mean and standard deviation of 5.1 mm and 5.8 mm respectively.

The small wavelength cellularity observable in Figure 2 has been investigated using OH PLIF. The results indicate that a small wavelength cellular structure is imbedded within the larger wavelength cellular structure. This is shown in the OH PLIF image reproduced in Figure 5 below.

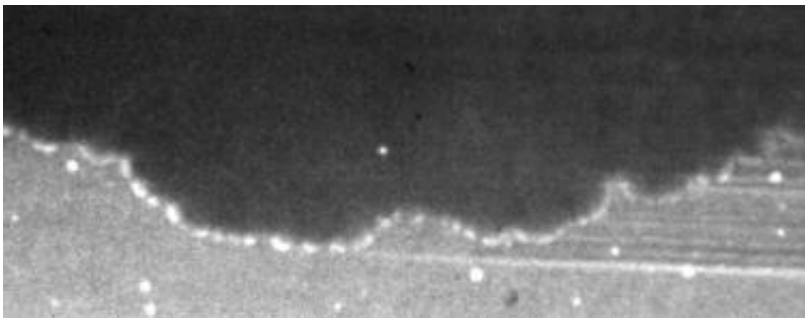

Figure 5: PLIF image showing the large and small wavelength cellularity for a 5 bar, ϕ = 1.4, iso-octane-air explosion flame [3, 4]. (Flame radius ≈ 60mm, horizontal scale ≈ 55mm).

The continuous signal across the bottom of the image was produced by Rayleigh scattering from the unburned mixture ahead of the flame front at 308.24 nm. The continuous low signal across the top of the image represents fluorescence emitted from equilibrium OH, and Rayleigh scattering from the combustion gases behind the flame front. The bright spotty signals across the middle of the image represent regions of super-equilibrium OH in the textured flame front. The bright spots indicate regions of large rates of flame reaction rate, surrounded by regions of low flame reaction rate in the flame front. The small wavelength cellularity observable in Figure 5 has been subjected to a length-scale analysis, the results of which are shown in Figure 6 below. These smaller cells have planar cell lengths in the range of 0.5 mm to 2.5 mm.

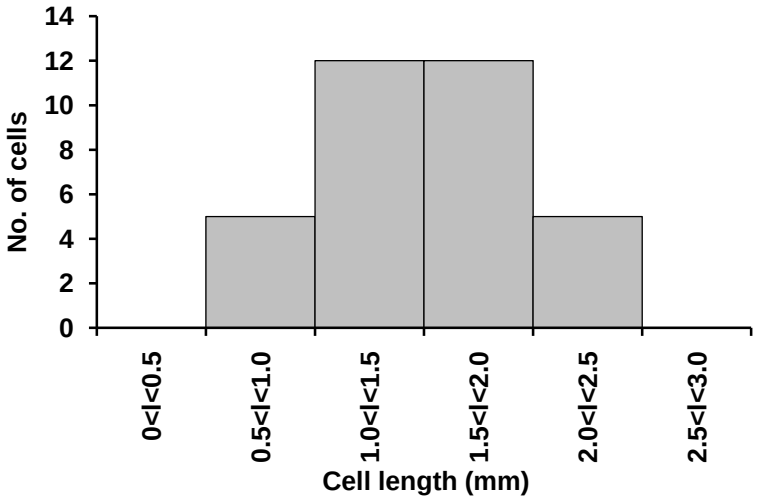

Figure 6: Histogram showing planar cell-size distribution obtained from Figure 5.

The planar length scale distribution (as shown in Figure 6) can be employed to derive the distribution of cell wavelengths, assuming the cells retain a regular surface structure (square, pentagonal, hexagonal, or circular, for example) [5]. Assuming the original cells shown in Figure 5 were circular in shape, the derived small wavelength distribution is shown in Figure 7. This distribution of small cell wavelengths has a mean wavelength of 1.6 mm, and a standard deviation of 0.4 mm.

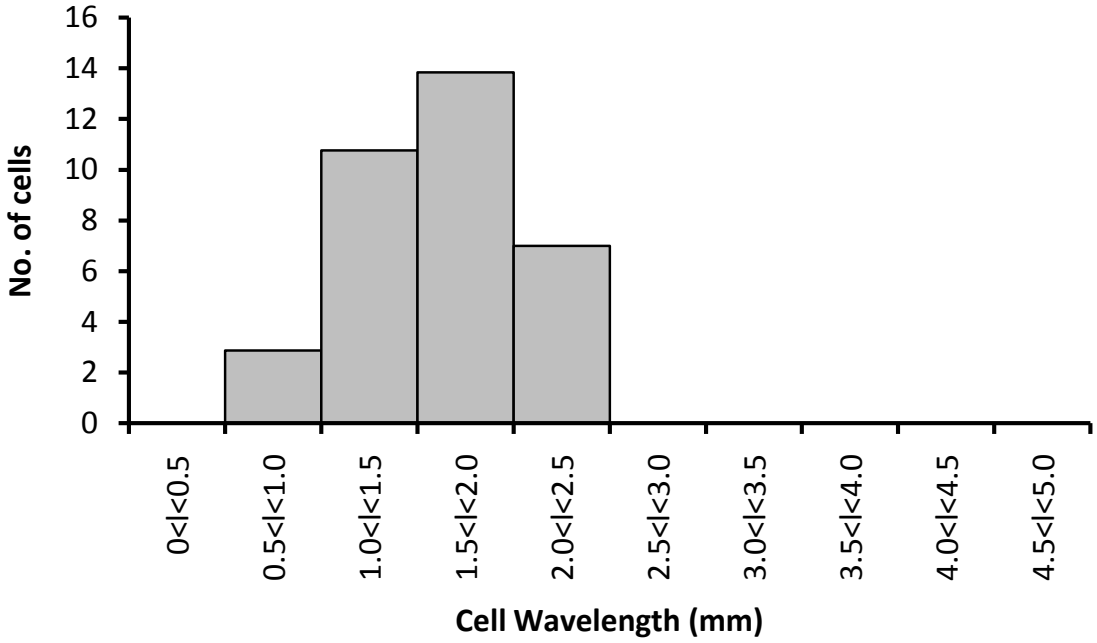

Figure 7: Histogram of small cell wavelengths, derived from Figure 6.

4. Discussion

Figure 1 shows the development of a large wavelength cellularity on the flame surface. The interior surface within the cell boundaries appears to be smooth and continuous. The thermal-diffusive instability couples to the hydrodynamic instability, enabling the development of the large wavelength cellularity.

In contrast, Figure 2 shows the development of a small wavelength textured surface imbedded within large wavelength cellularity. The observation that the large wavelength cellularity is present in both explosion flames suggests that the mechanism responsible for the development of the cellularity is the same in both cases. This suggests that the hydrodynamic instability dominated the mechanism responsible for the large wavelength instability.

This argument is supported by the histograms shown in Figures 3 and 4, which reveal that the distributions of large cell wavelengths is similar for the two combustion cases (stoichiometric and $\phi = 1.4$), with similar means and standard deviations.

The OH PLIF image shown in Figure 5 reveals the detailed structure of the flame surface. The image shows small wavelength flame structures imbedded within the larger wavelength cellularity. The OH fluorescence image reveals regions of large reaction rate adjacent to regions of small reaction rate. This is the flame structure expected of a flame subject to the thermal diffusive instability [2, 6]. It is therefore suggested that the small wavelength structure is a

consequence of the thermal-diffusive instability.

The histograms presented in Figures 4, 5, and 7, together with the image data (as represented in Figures 1 – 3) suggest that a dual wavelength cellularity co-exists on the $\phi = 1.4$ explosion flame, developing independently as the flame expands. The large wavelength cells appear to contain approximately 15 – 40 smaller wavelength cells, depending on the relative size of the large and small cells.

The small wavelength structure of the rich explosion flame makes it difficult to relate global flame surface measurements of laminar burning velocity to local fuel oxidation processes in the textured flame surface. Detailed flame structure calculations including small scale dynamics are required to reconcile global measurements with local flame dynamics.

5. Conclusions

1. Schlieren cinematography of stoichiometric and rich 5 bar iso-octane-air laminar explosion flames reveal the development of cellular structure. In addition, the $\phi = 1.4$ explosion flame exhibits a small wavelength structure on the flame surface.

2. Cell-size distributions have been obtained from the stoichiometric and rich explosion flames. The distributions indicate similar means and moments. This suggests that this large wavelength cellularity is caused by the hydrodynamic instability.

3. A smaller wavelength cellularity was observed to develop in the surface of the $\phi = 1.4$ explosion flame. This suggests that the small scale cellularity is caused by the thermal-diffusive instability.

4. Cellular structures with two different wavelengths can co-exist on a flame surface. This has implications for the determination of the laminar burning velocity of these explosion flames.

References

1. D. Bradley, C.M. Harper, *The development of instabilities in laminar explosion flames*, Proceedings of the Combustion Institute 25 (1994) 562 – 572.

2. D. Bradley, C.G.W. Sheppard, R. Woolley, D.A. Greenhalgh, R.D. Lockett, *The development and structure of flame instabilities and cellularity at low Markstein numbers in explosions*, Combustion and Flame 122 (2000) 195 – 209.

3. R.D. Lockett, *Instabilities and soot formation in spherically expanding, high pressure, rich, iso-octane-air flames*, Journal of Physics: Conference Series 45 (2006) 154–160.

4. R. Woolley, C.G.W. Sheppard, Unpublished work, University of Leeds, Leeds, UK (2005).

5. R.D. Lockett, to be published (2010).

6. G. Patnaik, K. Kailasanath, E.S. Oran, K.J. Laskey, *Detailed numerical simulations of cellular flames*, Proceedings of the Combustion Institute 22 (1989) 1517 - 1526.

Acknowledgements: The authors would like to acknowledge R. Woolley (presently Univ. of Sheffield) and C. Sheppard (Univ. of Leeds) for their contribution and assistance in supplying relevant, unpublished Schlieren data.